Cleaner Materials 18 (2025) 100349

Contents lists available at ScienceDirect

Cleaner Materials

journal homepage: www.journals.elsevier.com/cleaner-materials

New insights into value-added application of phosphogypsum in asphalt mixture through chemical stabilization of polymeric methylene diphenyl diisocyanate☆

Xiaomei Huang [a,b,c], Xiong Xu [a,b,c,*], Guohao Xu [a,b], Xiong Tao [d], Anand Sreeram [e], Zhifei Tan [f,g,*]

[a] School of Civil Engineering and Architecture, Wuhan Institute of Technology, Wuhan, China
[b] State Key Laboratory of Green and Efficient Development of Phosphorus Resources, Wuhan Institute of Technology, Wuhan, China
[c] Hubei Provincial Engineering Research Center for Green Civil Engineering Materials and Structures, Wuhan Institute of Technology, Wuhan, China
[d] Hubei Provincial Expressway Industrial Development Co., Ltd, Wuhan, China
[e] Nottingham Transportation Engineering Centre (NTEC), University of Nottingham, Nottingham, United Kingdom
[f] College of Architecture and Civil Engineering, Beijing University of Technology, Beijing, China
[g] Department of Civil and Environmental Engineering, The Hong Kong Polytechnic University, Hong Kong, China

ARTICLE INFO

Keywords:
Phosphogypsum
Asphalt mixtures
Freeze-thaw resistance
Fatigue resistance
Long-term performance

ABSTRACT

Phosphogypsum (PhG), a high-volume industrial byproduct, has considerable potential for use in asphalt mixtures. Its utilization is of great significance for mitigating the excessive consumption of natural mineral fillers. However, the high water absorption and wet expansion of PhG significantly compromise the moisture-induced resistance and durability of asphalt mixtures, thereby limiting its broader engineering application. In this study, PhG was used as a full replacement for conventional mineral filler, and polymeric methylene diphenyl diisocyanate (PMDI) was introduced as an asphalt binder modifier to prepare PhG asphalt mixtures (PhGAM). The fatigue and freeze-thaw (F-T) resistance of PhGAM were evaluated using semicircular bending (SCB) fatigue and F-T cycle tests, respectively. After simulating thermo-oxidative aging, the long-term service performance of PhGAM was systematically assessed through wheel tracking, low-temperature indirect tensile, Marshall immersion, and F-T cycling tests. The SCB test results demonstrated that 4% PMDI, by weight of asphalt binder, can markedly improve the fatigue life of PhGAM, whereas further increasing PMDI content provides limited additional benefit. F-T cycle test results indicated that the incorporation of PMDI can notably enhance the indirect tensile strength and water damage resistance of PhGAM, enabling it to withstand at least four cycles, whereas the unmodified PhGAM/PMDI0 fails after only one. After long-term aging, aged PhGAM/PMDI mixtures exhibit significantly higher resistances to permanent deformation at elevated temperature compared to unaged ones. The dynamic stability of aged PhGAM/PMDI4 reaches 5736 passes/mm, compared to 2921 passes/mm for aged PhGAM/PMDI0. Furthermore, aged PhGAM/PMDI4 still exhibits better resistance to low-temperature cracking and moisture-induced damage, especially compared to aged PhGAM/PMDI0. Overall, a 4 % PMDI content is optimally recommended for blending with the asphalt binder for enhancing the engineering performance of PhGAM and facilitating the high-value utilization of PhG in the construction of more durable asphalt pavement.

1. Introduction

Asphalt mixtures are widely used in pavement engineering due to their viscoelastic nature and favorable mechanical properties (Cheng et al. 2016, Wu et al. 2021, Xu et al. 2021). They are typically composed of asphalt binder, aggregates, and mineral fillers in defined proportions (Chen et al. 2022, Xing et al. 2024). With the ongoing expansion of transportation infrastructure and the aging of existing pavements, the demand for asphalt mixtures continues to grow, leading to greater exploitation of non-renewable mineral resources such as limestone,

☆ This article is part of a special issue entitled: 'Pavement materials' published in Cleaner Materials.

* Corresponding authors.
E-mail addresses: xxucea@wit.edu.cn (X. Xu), zhifeitan@gmail.com (Z. Tan).

https://doi.org/10.1016/j.clema.2025.100349
Received 25 July 2025; Received in revised form 7 October 2025; Accepted 7 October 2025
Available online 11 October 2025

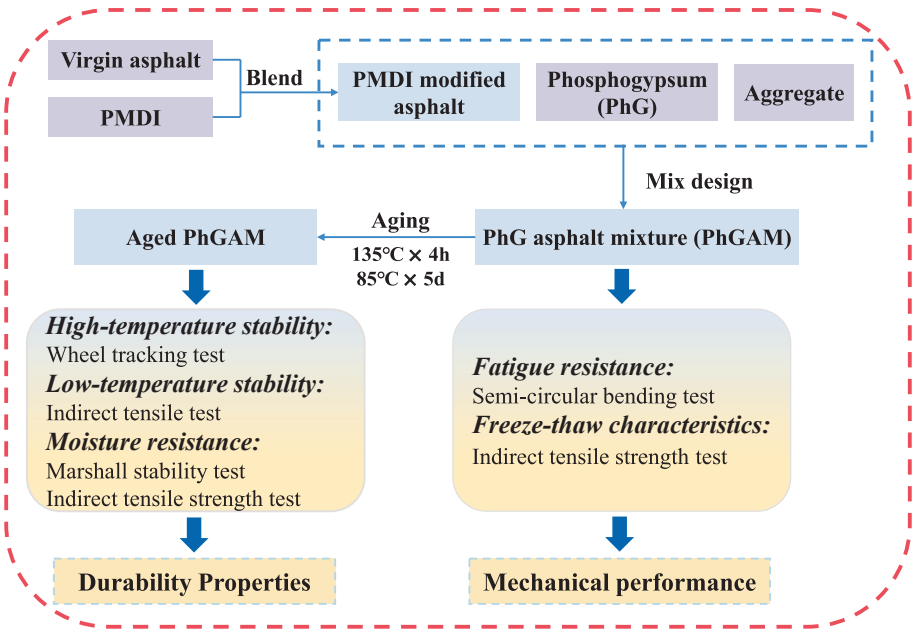

Fig. 1. Flowchart illustrating the research framework.

granite, and basalt (Xu et al. 2019). Although fillers represent a relatively small fraction of the mixture by mass, they play a vital role in improving mixture stiffness, enhancing asphalt-aggregate adhesion, and increasing durability (Chen et al. 2008, Wang et al. 2011). The long-term and large-scale mining of natural fillers not only depletes resources but also causes significant ecological damage (Zhang et al. 2018). As a result, industrial solid wastes including red mud, steel slag, and fly ash have found widespread application as substitute fillers in asphalt mixtures (Sun et al. 2023, Tan et al. 2025, Woszuk et al. 2019). Research has shown that fillers such as red mud and steel slag significantly improve the properties of asphalt mastic, which in turn enhances the overall performance of the related asphalt mixtures (Luo et al. 2025, Pereira et al. 2018). Therefore, the substitution of conventional mineral fillers with industrial solid wastes has become a significant research focus to promote sustainability in pavement engineering.

Phosphogypsum (PhG) is a major industrial byproduct generated from the wet-process production of phosphoric acid, with approximately 4.5–5 tons of PhG produced per ton of phosphate fertilizer (Baolin et al. 2022, Murali and Azab 2023, Zhang, L. et al. 2025). In China, the annual production of PhG exceeds 80 million tons, yet a large proportion remains insufficiently utilized (Shi et al. 2024). The extensive accumulation of PhG in large stockpiles consumes considerable land resources and poses environmental hazards. Harmful elements such as phosphorus and fluorine can leach out, thereby threatening soil and groundwater quality (Bilal et al. 2023, Cao et al. 2022, Qu et al. 2025). Therefore, its sustainable utilization is of considerable environmental and engineering significance.

Within this context, researchers have increasingly focused on the resource-efficient and volume-reducing utilization of PhG in asphalt mixtures (Zhang, L. et al. 2025, Zhang, X. et al. 2025). Existing studies have demonstrated promising potential for PhG as both an aggregate and filler in asphalt systems (Gong et al. 2024, Ou et al. 2023, Yin et al. 2024). For instance, Liu et al. (2022) used disc granulation and jaw crushing to produce PhG-based artificial aggregates, which proved feasible for partially replacing natural aggregates in asphalt mixtures. Similarly, Amrani et al. (2020) evaluated PhG alongside fly ash and dry phosphatic sludge as asphalt fillers, finding that PhG-based paste exhibited superior mechanical properties and rutting resistance relative to the other fillers. Furthermore, Mehta et al. (2020) employed a PhG-cement composite filler, which significantly enhanced the Marshall stability of the asphalt mixtures. However, due to its high water absorption and moisture-induced expansion, PhG tends to increase air void content and reduce volumetric stability in asphalt mixtures (Chen et al. 2024, Jin et al. 2025). These effects lead to increased moisture susceptibility and deterioration in mechanical performance, ultimately limiting the long-term durability of PhG asphalt mixtures (Arbabpour Bidgoli et al. 2019, Liang et al. 2023).

Polyethylene diphenyl diisocyanate (PMDI) is a highly reactive isocyanate compound whose terminal –NCO groups can react with hydroxyl and carboxyl groups in asphalt, including water molecules (H_2O), thereby enhancing the adhesion, moisture resistance, and aging resistance of polymer-modified asphalt binders (Cao et al. 2020, Xu et al. 2022, Zhang, Z. et al. 2025). For example, Zhang et al. (2024) developed an innovative modifier through the reaction of polypropylene glycol with MDI, resulting in notable enhancements in asphalt's high-temperature stability, low-temperature flexibility, and resistance to aging. Similarly, Li, Z. et al. (2021) demonstrated that polyurethane creates a three-dimensional network within the asphalt matrix, significantly improving resistance to high-temperature deformation, low-temperature cracking, and aggregate adhesion. Moreover, our previous study found that in PhG mixtures modified with PMDI, the isocyanate groups in PMDI react with water released from the PhG and hydroxyl groups on the aggregate surface, forming a cross-linked network that significantly enhances the moisture resistance of the mixture (Xu et al. 2025). However, the extent to which PMDI can mitigate the long-term durability issues associated with PhG incorporation remains unclear.

To overcome this limitation, the present study introduces the application of PMDI-modified asphalt in conjunction with PhG as a complete substitute for traditional fillers in the fabrication of PhG asphalt mixtures (PhGAM). The fatigue resistance and freeze-thaw (F-T) durability of PhGAM will be evaluated respectively through semicircular bending and freeze-thaw cycling tests. To assess long-term performance under simulated service conditions, rutting, low-temperature indirect tensile, Marshall immersion, and F-T indirect tensile strength will be conducted after thermo-oxidative aging. This study aims to systematically investigate the effectiveness of PMDI in enhancing the structural integrity and durability of PhGAM, providing theoretical and practical guidance for the high-value utilization of PhG in asphalt pavement applications. More importantly, it also promotes the resource-efficient

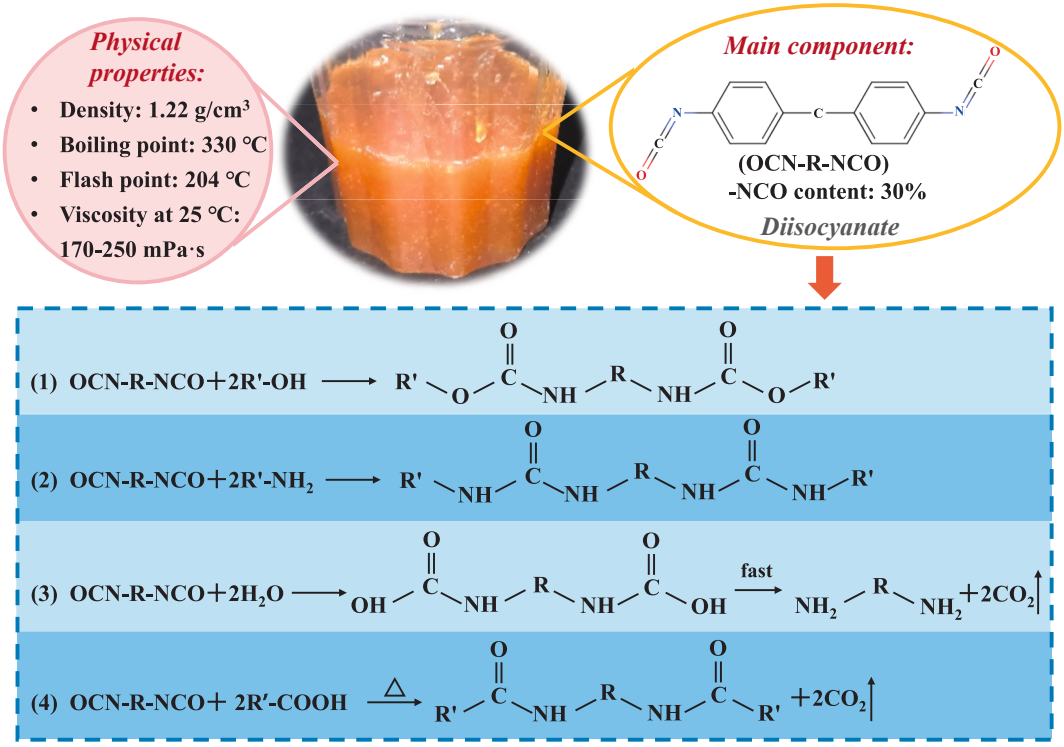

Fig. 2. Apparent morphology, physical properties and representative reaction equations of PMDI.

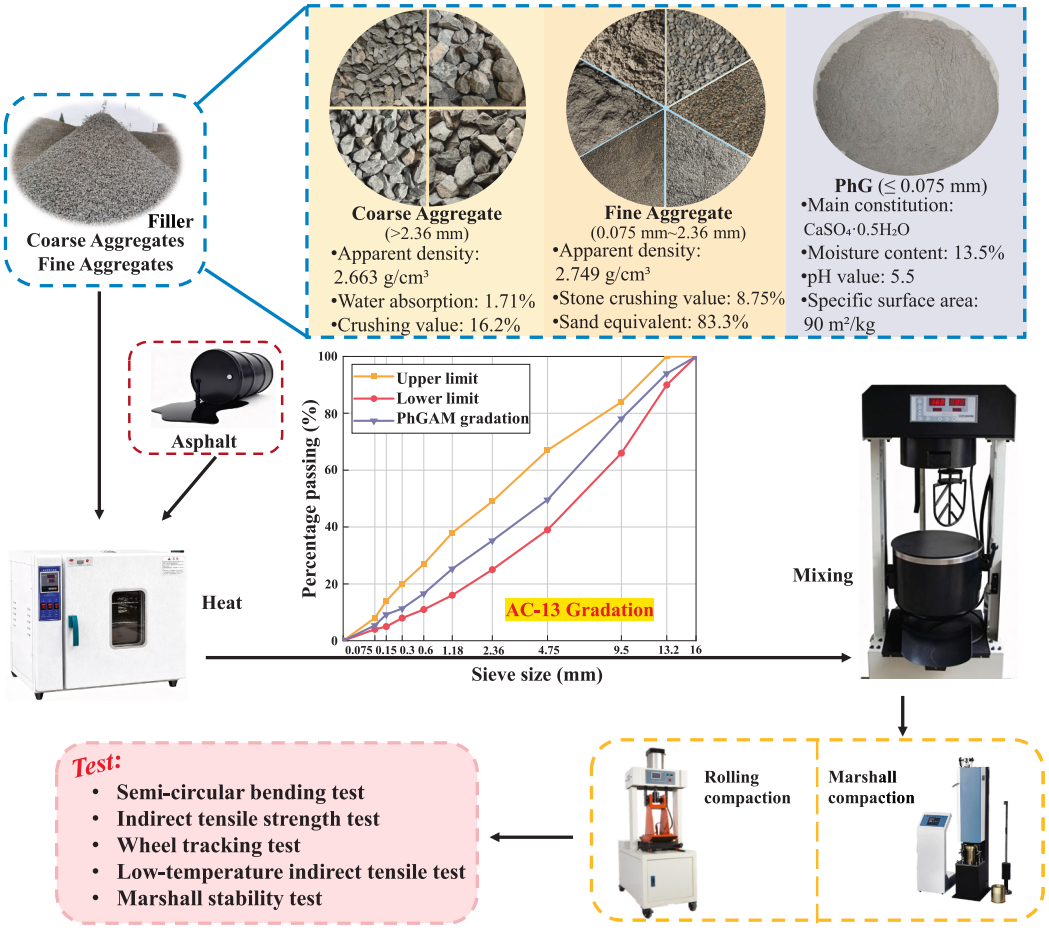

Fig. 3. Procedures for PhGAM preparation and specimen fabrication.

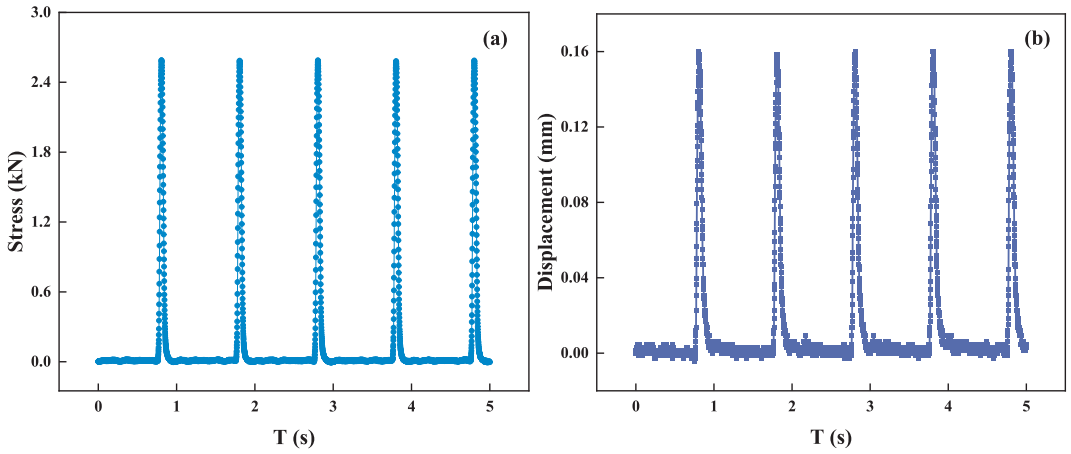

Fig. 4. Stress–time (a) and displacement–time (b) responses of SCB under cyclic loading.

utilization of industrial byproducts and advances cleaner material strategies, thereby contributing to sustainability in pavement engineering. The schematic of the overall research methodology is presented in Fig. 1.

2. Materials and methodologies

2.1. Raw materials

2.1.1. Virgin asphalt

The virgin asphalt binder employed in this study was a Penetration Grade 70 (Pen. 70) binder, procured from a local manufacturer in Wuhan. Key technical parameters of the binder included a softening point of 48.5 °C, a penetration of 68 (0.1 mm) at 25 °C, and ductility exceeding 100 cm at 15 °C.

2.1.2. Polymeric methylene diphenyl diisocyanate (PMDI)

The PMDI used in this study was obtained from a local chemical manufacturer in Wuhan, China. It consists of a mixture of monomeric MDI (two-ring structure) and polymeric MDI (three-ring or higher structures). Owing to its distinctive molecular configuration, PMDI can readily react with water, carboxyl groups, amines, and hydroxyl groups (Xu et al. 2025). The morphology, physical properties, and representative reaction mechanisms of PMDI are shown in Fig. 2.

2.1.3. Preparation of PhG asphalt mixture (PhGAM)

Natural limestone provided by Wuhan Zhongjian Commercial Concrete Co., Ltd. was used as coarse and fine aggregates, while phosphogypsum (PhG) obtained from a local phosphate fertilizer plant was employed as filler. Before use, the PhG was calcined at 160 °C for 4 h, washed, dried, and sieved through a 0.075 mm mesh.

In this study, the widely used AC-13 asphalt mixture gradation was selected. Specimens were prepared according to the Marshall design, and the key volumetric parameters were measured as follows: the voids in mineral aggregate (VMA) were approximately 15.8 %, air voids (Vv) were approximately 4.2 %, and voids filled with asphalt (VFA) were approximately 73.5 %. Considering the Marshall loads, the optimum asphalt content of PhGAM was determined to be 4.9 %. The preparation procedures of PhGAM and specimen fabrication are shown in Fig. 3. Specifically, PMDI was incorporated into the virgin asphalt binder at dosages of 2 %, 4 %, and 6 % by binder weight, and the mixture was sheared at 160 °C and 4000 rpm for 30 min. Subsequently, aggregates, modified binder, and PhG were sequentially added to a preheated mixing vessel at 180 °C and mixed for 15 s, 20 s, and 90 s, respectively. According to the PMDI content, the mixtures were denoted as PhGAM/PMDI0, PhGAM/PMDI2, PhGAM/PMDI4, and PhGAM/PMDI6.

Table 1
Failure load and corresponding stress of PhGAM at different stress ratios.

Item	*P*	0.2	0.3	0.4	0.5	0.6
PhGAM/PMDI0	6.44	1.01	1.47	1.95	2.44	2.93
PhGAM/PMDI2	7.95	1.21	1.81	2.41	3.01	3.62
PhGAM/PMDI4	8.66	1.31	1.97	2.62	3.28	3.94
PhGAM/PMDI6	8.20	1.24	1.86	2.49	3.11	3.73

2.1.4. Preparation of aged PhGAM

2.1.4.1. Short-term aging. According to ASTM D6521, short-term aging of the asphalt mixture was conducted using a thermo-oxidative aging method. The uniformly mixed PhGAM was evenly spread on enamel trays at a loose paving density between 21 and 22 kg/m^2, then placed into a ventilated oven maintained at 135 ℃ for 4 h. To guarantee uniform aging, the mixtures were stirred every hour during the heating process.

2.1.4.1. Long-term aging. The short-term aged PhGAM was compacted into standard Marshall specimens with dimensions of Ø101.6 mm × 63.5 mm and allowed to cool at room temperature for at least 16 h before demolding. Subsequently, the specimens were placed in an oven at 85 °C and aged continuously for 5 d. After aging, they were removed and conditioned at room temperature for 16 h to obtain the long-term aged PhGAM.

2.2. Semi-circular bending (SCB) test

The fatigue behavior of PhGAM was evaluated by SCB tests at intermediate temperature using a UTM-100 system. The procedure was as follows: (1) standard Marshall specimens were sliced vertically to obtain semi-cylindrical samples, and a pre-cut notch measuring 10 mm × 1.5 mm was introduced at the midpoint of the flat bottom surface; (2) an indirect tensile test was performed to determine the maximum failure load (*P*); (3) the nominal tensile stress (σ_t) at the bottom of the specimen was calculated using Equation (1) to determine the stress levels for the cyclic SCB fatigue test (Bui and Saleh 2021, Teixeira et al. 2023); and (4) cyclic loading was applied in stress-controlled mode at 15 °C using a 10 Hz half-sine waveform. Stress ratios of 0.2, 0.3, 0.4, 0.5, and 0.6 were tested, and the corresponding fatigue life (N_f) was recorded for each specimen. Under stress-controlled loading, cracks propagated along the pre-cut notch, gradually reducing the effective load-bearing area. The applied load increased to maintain the nominal stress until failure, reflecting progressive fatigue damage accumulation. At least three specimens were tested for each stress level. Typical stress–time and

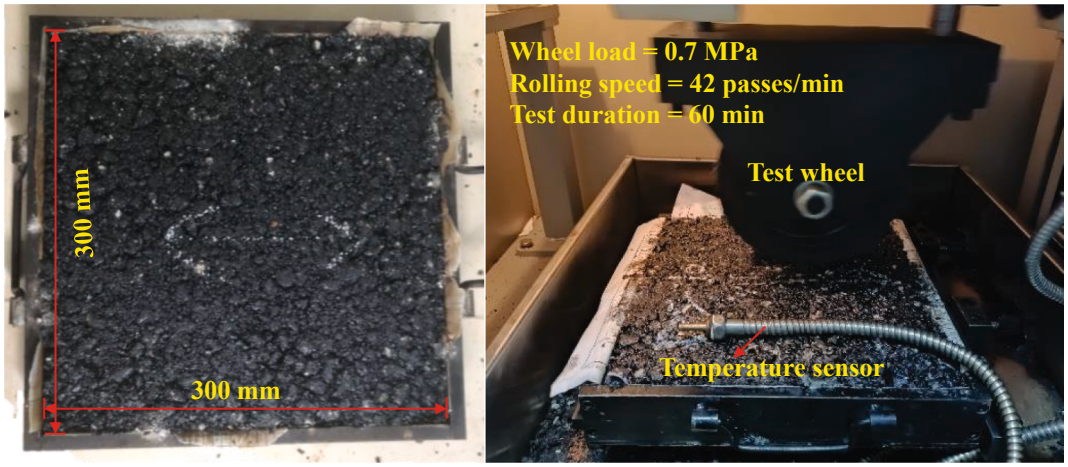

Fig. 5. Rutting specimen and wheel tracking test setup.

displacement–time responses of SCB specimens under cyclic loading are shown in Fig. 4, and Table 1 summarizes the nominal tensile stresses and corresponding failure loads at different stress ratios.

$$\sigma_t = \frac{4.8P}{DW} \tag{1}$$

where, D is the specimen diameter, mm; and W is the specimen width, mm.

Given the variation in fracture strength among different specimen groups, the fatigue performance of PhGAM cannot be adequately assessed using fatigue life alone. Therefore, the fatigue behavior of PhGAM with varying PMDI contents was quantitatively evaluated using the logarithmic fatigue relationship (see Equation (2)), where the fitted parameters served as indicators of fatigue resistance (Gao et al. 2016).

$$lgN_f = n - klg\sigma \tag{2}$$

where, n denotes the intercept and k represents the slope of the curve; and a higher k value indicates increased susceptibility of the mixture to load variations.

2.3. Indirect tensile strength (ITS) test

The ITS test was employed to evaluate the freeze-thaw (F–T) resistance of PhGAM under different aging and F-T conditions. Unaged PhGAM specimens underwent 1–5 F-T cycles, whereas aged PhGAM specimens underwent one cycle. According to AASHTO T283, each F-T cycle included the following steps: (1) vacuum saturation of the specimens; (2) specimens were frozen at –18 °C for 16 h, then thawed in a water bath maintained at 60 °C for 24 h; and (3) conditioned in a 25 °C water bath for 2 h. The tensile strength ratio (*TSR*) was determined according to Equation (3) to evaluate the changes in ITS of PhGAM after these treatments. Three sets of replicate samples were tested under each condition to ensure the reliability of the data.

$$TSR = \frac{ITS_i}{ITS_0} \times 100\% \tag{3}$$

where, *TSR* represents the tensile strength ratio after i F-T cycles, %; ITS_i represents the ITS after i F-T cycles, MPa; and ITS_0 represents the ITS of unaged PhGAM/PMDI0 without F-T cycling, MPa. This definition allows a clearer assessment of the effect of PMDI content on the F-T performance of PhGAM, rather than solely reflecting damage caused by F-T cycles.

2.4. Wheel tracking test

In this study, the wheel tracking test was employed to evaluate the effect of long-term aging on the high-temperature performance of PhGAM. According to ASTM D8292, slab specimens measuring 300 mm × 300 mm × 50 mm were conditioned in a chamber at 60 °C for 5 h. Wheel-tracking tests were then conducted under a wheel load of 0.7 MPa at a rolling speed of 42 passes/min for 60 min. The rutting specimens and the test setup are shown in Fig. 5. The rut depth (RD) of each specimen was continuously recorded throughout the test. Three replicate tests were conducted on specimens with the same mix ratio to ensure the accuracy of the test data. The rate of RD development was determined by computing the first derivative of the RD curve with respect to loading time, serving as an indicator of the mixture's susceptibility to permanent deformation at elevated temperatures. Dynamic stability (DS) was then calculated following Equation (4), where higher DS values reflect enhanced resistance to high-temperature

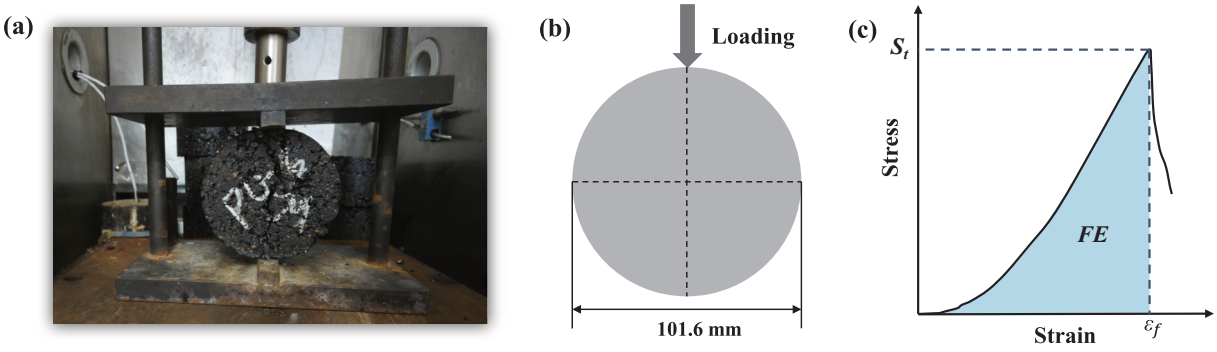

Fig. 6. Schematic of IDT test: (a) loading process, (b) loading schematic, and (c) *FE* schematic.

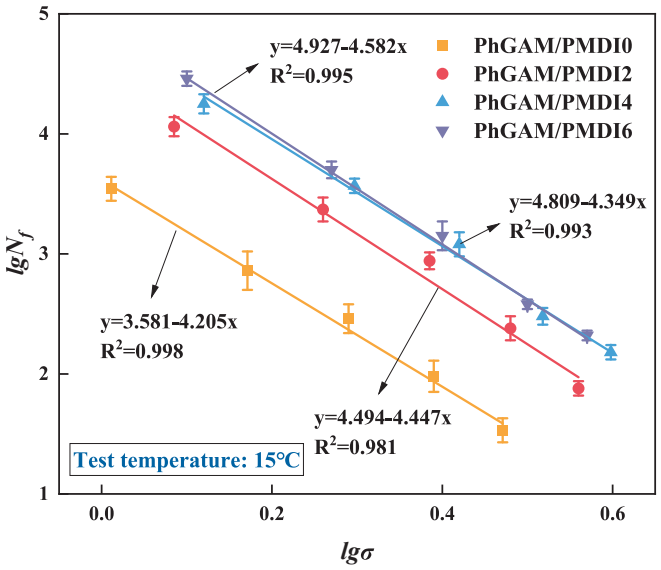

Fig. 7. The fatigue curves of PhGAM/PMDI.

deformation.

$$DS = \frac{(t_2\text{-}t_1) \times N}{d_2\text{-}d_1} \times C_1 \times C_2 \quad (4)$$

where, d_1 and d_2 are the rut depths measured at 45 min (t_1) and 60 min (t_2), respectively; N is the rolling frequency of the test wheel (pass/min); and C_1 and C_2 are correction coefficients related to the device and specimen, typically taken as 1.0.

2.5. Low-temperature indirect tensile (IDT) test

The IDT test was employed to evaluate the effect of long-term aging on the low-temperature cracking resistance of PhGAM. According to T0716-2011 specified in JTG E20-2011, specimens were conditioned at −10 °C for 4 h prior to testing. A compressive load was applied at a constant rate of 1 mm/min until failure, while the load–displacement curve was continuously recorded. At least three specimens were tested under each condition to ensure data reproducibility. The indirect tensile strength (R_T), Poisson's ratio (μ), failure stiffness modulus (S_T), and fracture energy (*FE*) were calculated according to Equations (5)–(8). The loading procedure and a schematic of *FE* calculation are illustrated in Fig. 6.

$$R_T = 0.006287P_T/h \quad (5)$$

$$\mu = (0.1350A - 1.7940)/(-0.5A - 0.0314) \quad (6)$$

$$S_T = P_T \times (0.27 + 1.0\mu)/(h \times X_T) \quad (7)$$

$$FE = \int_0^{\varepsilon_f} S(\varepsilon)\cdot d\varepsilon \quad (8)$$

where, P_T is the load at specimen failure, N; h is the specimen height, mm; A is the ratio between vertical and horizontal deformation, defined as $A = Y_T/X_T$; Y_T is the total vertical deformation of the specimen at maximum failure load, mm; X_T is the total vertical deformation at the peak failure load, mm; *St* indicates the maximum fracture stress expressed, MPa; $\hat{I}\mu_f$ is the fracture strain corresponding to the peak fracture stress, %.

2.6. Marshall stability (MS) test

The moisture damage resistance of aged PhGAM was assessed using the MS test. According to ASTM D6927-15, aged PhGAM specimens were subjected to two conditioning procedures: one set was soaked in a 60 °C water bath for 30 min, and another set was soaked in water for 48 h. Both sets were then subjected to MS testing at a loading rate of 50 mm/min, with each set including no fewer than three replicate specimens. Residual Marshall Stability (RMS) was then determined based on Equation (9), where higher RMS values indicate enhanced moisture resistance of the asphalt mixture.

$$RMS = \frac{MS_1}{MS} \times 100\% \quad (9)$$

where, MS_1 is the Marshall load of aged specimens following immersion for either 30 min or 48 h immersion, kN; and *MS* is the Marshall load of unaged PhGAM/PMDI0 specimens immersed for 30 min, kN.

Table 2
The fatigue curve equation of PhGAM/PMDI.

Item	Fatigue equation	n	k	R^2
PhGAM/PMDI0	$lgN_f = 3.581–4.205lg\sigma$	3.581	4.205	0.988
PhGAM/PMDI2	$lgN_f = 4.494–4.447lg\sigma$	4.494	4.447	0.981
PhGAM/PMDI4	$lgN_f = 4.809–4.349lg\sigma$	4.809	4.349	0.993
PhGAM/PMDI6	$lgN_f = 4.927–4.592lg\sigma$	4.927	4.592	0.995

3. Results and discussion

3.1. Fatigue resistance

Fig. 7 displays the fitted curves showing the fatigue life of PhGAM/PMDI. The fatigue lives decrease with increasing stress level, indicating that higher loads are more likely to induce fatigue failure of the mixture. Moreover, as PMDI content increases from 0 % to 6 %, the lgN_f value of the PhGAM first goes up and then stabilizes within the applied stresses. Notably, PhGAM/PMDI4 and PhGAM/PMDI6 show a comparable fatigue performance. These results indicated that PMDI effectively improves the fatigue resistance of PhGAM, while the effect is limited when PMDI content exceeds 4 %. This is mainly attributed to PMDI chemically improving the asphalt binder's elasticity and deformation recovery, which reduces microcrack initiation under repeated loading and slows the propagation of existing cracks (Khairuddin et al. 2019).

Table 2 presents the corresponding fitted fatigue equations and correlation coefficients (R^2) of PhGAM/PMDI. All fitted equations exhibit R^2 values exceeding 0.980, demonstrating a high accuracy and reliability. As shown, PhGAM/PMDI0, PhGAM/PMDI2, PhGAM/PMDI4, and PhGAM/PMDI6 have similar *k* values of 4.205, 4.447, 4.349, and 4.592, respectively, with corresponding *n* values of 3.581, 4.494, 4.809, and 4.927. These results demonstrated that an appropriate amount of PMDI can help maximize the anti-fatigue improvement of PhGAM and does not cause a significant increase in susceptibility of PhGAM to repeated loads in fatigue damage.

3.2. F-T resistance

Fig. 8 illustrates the F-T resistance of PhGAM/PMDI. As shown in Fig. 8(a), with increasing F-T cycles, the ITS of PhGAM gradually declines, whereas under identical conditions, ITS rises with higher PMDI content. Across all F-T cycles, PhGAM/PMDI0 consistently exhibits the lowest ITS values, while PhGAM/PMDI6 shows the highest ITS. Compared with PhGAM/PMDI0, PhGAM/PMDI2, PhGAM/PMDI4, and PhGAM/PMDI6 exhibit ITS values that are 18–25 % higher prior to F-T exposure and remain 29–55 % higher after five F-T cycles. The findings indicated that the PMDI markedly improves the mechanical performance and F-T resistance of PhGAM, which in turn contributes to its enhanced durability against long-term moisture-related deterioration. This enhancement is mainly attributed to the high chemical activity of the isocyanate groups (–NCO) in PMDI, which chemically react with

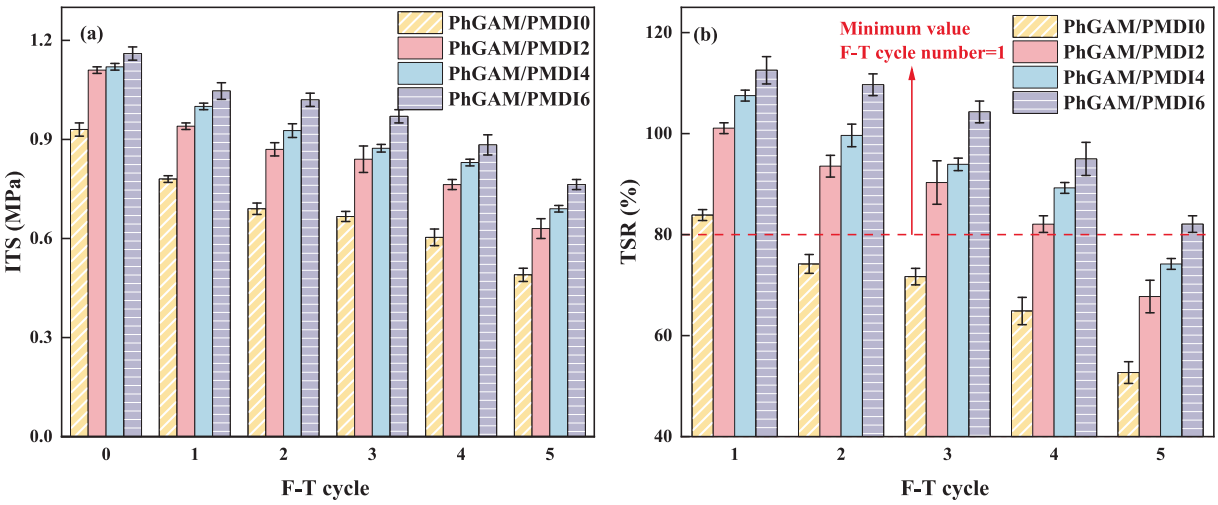

Fig. 8. F-T resistance of PhGAM/PMDI: (a) ITS and (b) TSR.

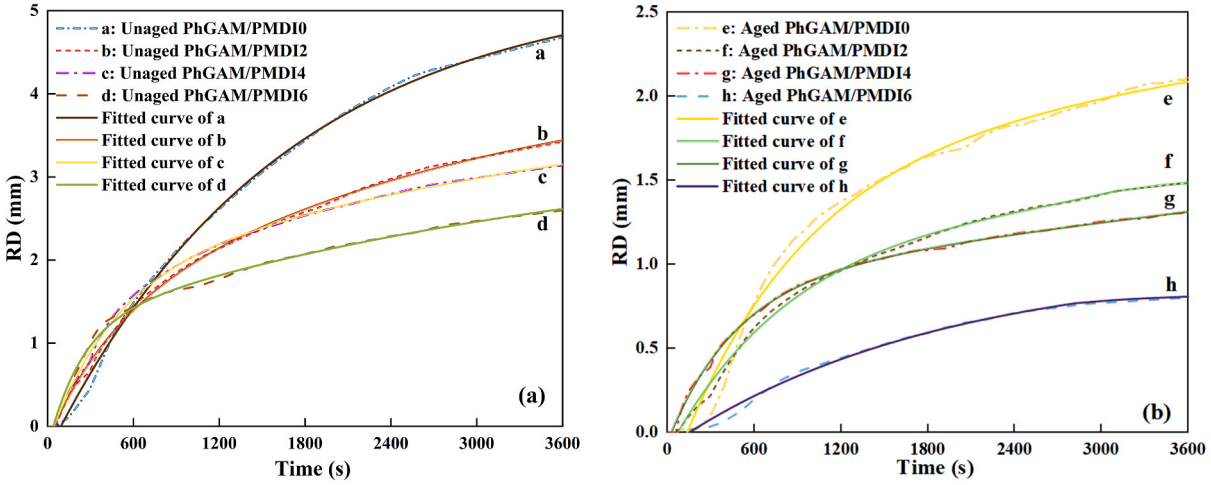

Fig. 9. RD of (a) unaged PhGAM/PMDI and (b) aged PhGAM/PMDI at 60 ℃.

functional groups in the asphalt binder that contain active hydrogen, including hydroxyl and carboxyl groups (Xia et al. 2016), thereby strengthening the binder-aggregate interfacial adhesion.

As demonstrated in Fig. 8(b), "Minimum TSR after 1 F-T cycle" indicates the minimum TSR value (80 %) that the asphalt mixture should achieve after the first F-T cycle, and all mixtures meet this requirement after one F-T cycle. The TSR of PhGAM gradually declines as the number of F-T cycles increases. After two F-T cycles, the TSR value of PhGAM/PMDI0 drops below 80 %, whereas PhGAM/PMDI2, PhGAM/PMDI4, and PhGAM/PMDI6 remain above 80 % after four cycles, reaching 82 %, 89 %, and 95 %, respectively. Notably, TSR values occasionally exceed 100 %, indicating that PMDI-modified PhGAM retains higher strength than unmodified PhGAM/PMDI0 after F-T cycles. After five F-T cycles, the TSR value of PhGAM/PMDI6 decreases to 82 %, which still exceeds the required minimum threshold of 80 % and is approximately 55 % higher than that of PhGAM/PMDI0. These findings show that PhGAM/PMDI0 has poorer resistance to moisture-induced damage under F-T conditions, whereas the incorporation of PMDI significantly enhances performance retention. Furthermore, as the number of cycles increases, the performance advantage of PMDI-modified PhGAM becomes more pronounced, highlighting its superior environmental adaptability and durability.

Table 3
Fitted equation of RD change of aged PhGAM at 60 ℃.

Item	Fitted equation	R^2
a	$y = -e^{(-x/1620.61)} \times 2.83\text{-}e^{(-x/1620.66)} \times 2.79 + 5.32$	0.998
b	$y = -e^{(-x/464.07)} \times 1.33\text{-}e^{(-x/2984.37)} \times 3.24 + 4.41$	0.989
c	$y = -e^{(-x/447.82)} \times 1.89\text{-}e^{(-x/4288.45)} \times 2.56 + 4.26$	0.993
d	$y = -e^{(-x/233.82)} \times 1.45\text{-}e^{(-x/3846.73)} \times 2.33 + 3.53$	0.996
e	$y = -e^{(-x/464.07)} \times 1.33\text{-}e^{(-x/2984.37)} \times 3.24 + 4.41$	0.998
f	$y = -e^{(-x/877.44)} \times 1.99\text{-}e^{(-x/1468.27)} \times 1.72 + 1.72$	0.987
g	$y = -e^{(-x/463.65)} \times 0.93\text{-}e^{(-x/1344.15)} \times 1.83 + 2.71$	0.999
h	$y = -e^{(-x/913.02)} \times 1.45\text{-}e^{(-x/1063.72)} \times 0.63 + 1.33$	0.997

3.3. High-temperature performance

3.3.1. Rutting resistance

Fig. 9 presents the fitted RD curves of aged PhGAM/PMDI, with corresponding equations and main parameters listed in Table 3. These equations serve as the basis for calculating RD development rates, as discussed in Section 3.3.2. All fitted curves exhibit R^2 values exceeding 0.987, confirming that the models accurately represent the relationship between RD and the service life of PhGAM/PMDI mixtures. As clearly seen, compared to unaged PhGAM/PMDI mixtures, their corresponding aged ones have significantly lower RD values within the designed

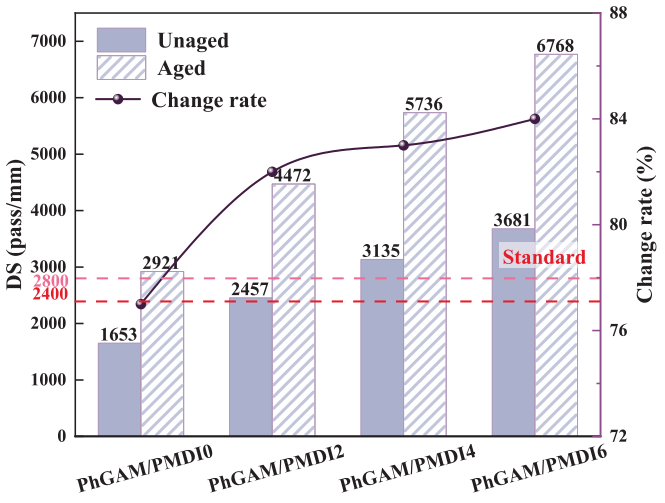

Fig. 10. DS of aged PhGAM/PMDI.

working time, suggesting that the thermal-oxidative aging can increase the high-temperature rutting resistance of PhGAM/PMDI, similar to the impact on common asphalt mixtures. When the working time reaches 3600 s, increasing the PMDI content from 0 % to 2 %, 4 %, and 6 % leads to a reduction in the RD of aged PhGAM/PMDI from 2.258 mm to 1.479 mm, 1.311 mm, and 0.814 mm, respectively. These results suggested that PMDI can effectively improve the high-temperature stability of aged PhGAM, thereby decreasing deformation under identical loading durations.

Fig. 10 shows the DS values of aged PhGAM/PMDI. With increasing PMDI content from 0 % to 2 %, 4 %, and 6 %, the DS value of unaged PhGAM/PMDI increases from 1653 passes/mm to 2457, 3135, and 3681 passes/mm, surpassing the technical requirement of 2400 passes/mm for PMDI-modified asphalt mixtures. These results indicated that unaged PhGAM is prone to rutting deformation under high-temperature conditions, while PMDI effectively enhances its high-temperature rutting resistance. After aging, the DS of PhGAM/PMDI rises from 2921 passes/mm to 6768 passes/mm as PMDI content increases from 0 % to 6 %, meeting the more stringent technical requirement of 2800 passes/mm. The corresponding DS change rates are 77 %, 82 %, 83 %, and 84 %, respectively. These results identified that thermal-oxidative aging improves the high-temperature rutting resistance of PhGAM, and the addition of PMDI further enhances its structural stability and resistance to permanent deformation. This improvement is attributed to the role of PMDI in enhancing the compactness and stability of the asphalt binder, thereby effectively reducing its flowability at elevated temperatures (Li, Z. et al., 2021). Moreover, after thermal-oxidative aging, the increased polar functional groups in the asphalt further promote the formation of a more stable structure, improving high-temperature stability (Zhang et al. 2024).

3.3.2. Rate of RD

To further analyze the RD development rate of aged PhGAM/PMDI, the derivative of the fitted RD curves in Fig. 9 was calculated. The resulting RD development rate curves before and after aging are shown in Fig. 11, with the corresponding regression equations and R^2 listed in Table 4. All R^2 values exceed 0.996, confirming that the fitted curves accurately characterize the relationship between RD development rate and working time. As presented in Fig. 11, the RD development rate of PhGAM/PMDI significantly decreased after aging, indicating that thermo-oxidative aging improved its high-temperature performance. After aging, PhGAM/PMDI0 consistently exhibits a relatively high RD development rate throughout the working process. Although PhGAM/PMDI2 shows some improvement, its development rate remains higher than those of PhGAM/PMDI4 and PhGAM/PMDI6. Notably, the RD development rate of PhGAM/PMDI4 is slightly higher than that of PhGAM/PMDI6 during the initial 900 s, after which the two rates converge. These results suggest that an appropriate PMDI content, particularly at 4 %, can effectively retard the rutting deformation of aged PhGAM. This is attributed to ongoing reactions between PMDI and polar functional groups in the asphalt binder during aging, forming a stable chemically cross-linked network (Jiang et al. 2024). Such a network restricts the mobility of the asphalt binder at elevated temperatures and effectively mitigates accelerated rutting deformation induced by long-term aging, thereby reducing the high-temperature susceptibility of PhGAM/PMDI.

Table 4
Fitted equation of RD development rate of aged PhGAM/PMDI at 60 ℃.

Item	Differential fitted equation	R^2
a	$y_1 = e^{(-x/1621.25)} \times 3.47 \times 10^{-3}$-$4.98 \times 10^{-7}$	0.997
b	$y_1 = e^{(-x/1322.46)} \times 2.68 \times 10^{-3}$-$8.32 \times 10^{-8}$	0.996
c	$y_1 = e^{(-x/996.32)} \times 3.09 \times 10^{-3}$-$1.02 \times 10^{-7}$	0.998
d	$y_1 = e^{(-x/984.68)} \times 2.62 \times 10^{-3}$-$1.84 \times 10^{-7}$	0.998
e	$y_1 = e^{(-x/603.45)} \times 3.41 \times 10^{-3}$-$4.47 \times 10^{-7}$	0.998
f	$y_1 = e^{(-x/877.49)} \times 2.27 \times 10^{-3}$-$1.17 \times 10^{-7}$	0.999
g	$y_1 = e^{(-x/472.39)} \times 2.03 \times 10^{-3}$-$1.14 \times 10^{-7}$	0.997
h	$y_1 = e^{(-x/915.19)} \times 1.50 \times 10^{-3}$-$1.09 \times 10^{-7}$	0.998

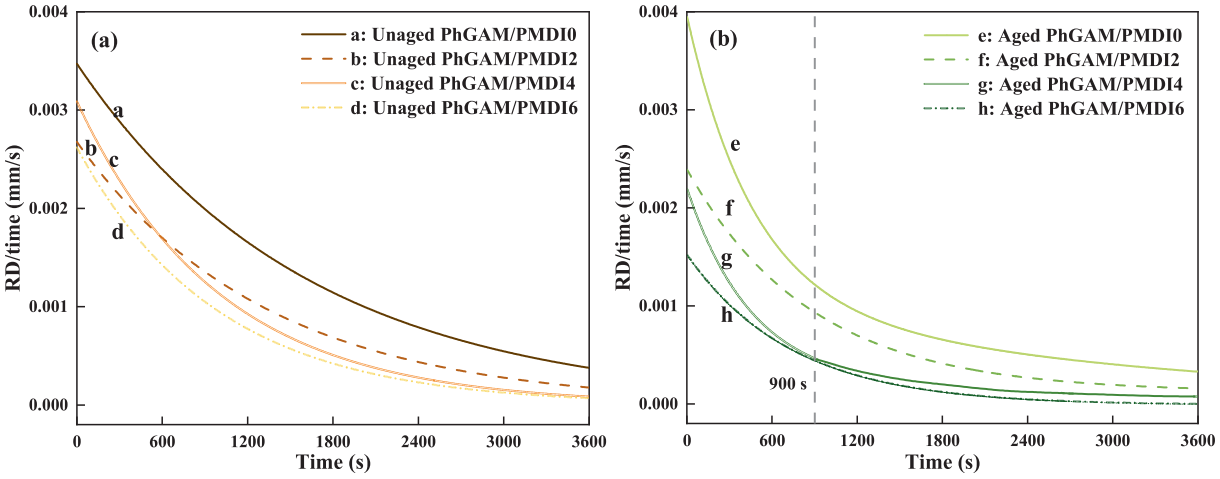

Fig. 11. RD development rate of (a) unaged PhGAM/PMDI and (b) aged PhGAM/PMDI.

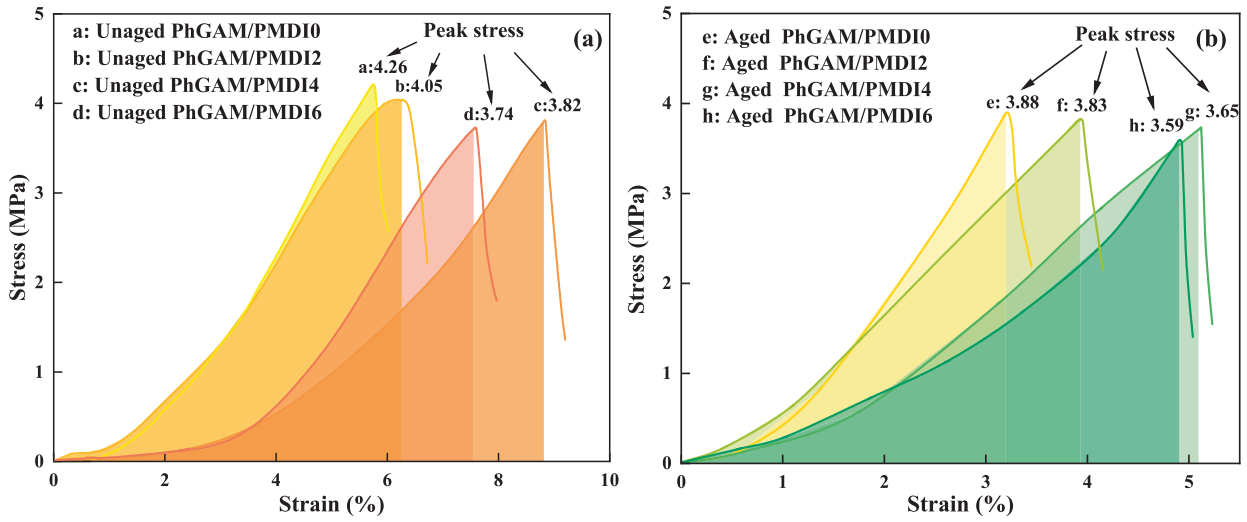

Fig. 12. Stress–strain and FE curves of (a) unaged PhGAM/PMDI and (b) aged PhGAM/PMDI.

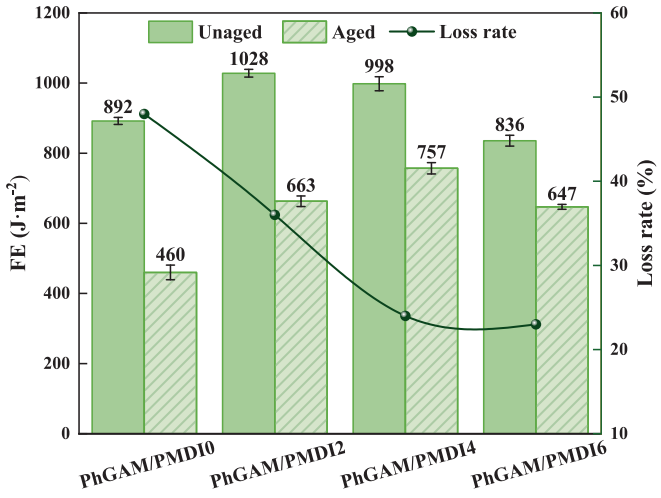

Fig. 13. FE of aged PhGAM/PMDI.

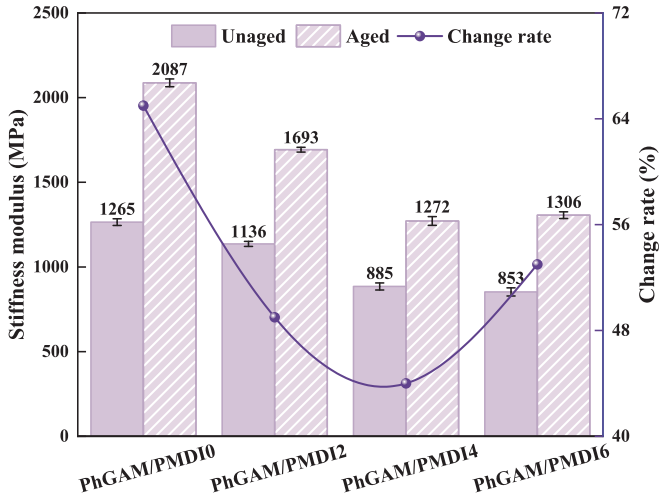

Fig. 14. Stiffness modulus of aged PhGAM/PMDI.

3.4. Low-temperature performance

3.4.1. Stress–strain curve

Fig. 12 presents the stress–strain and FE curves of long-term aged PhGAM/PMDI. It can be seen that both the peak stress and the corresponding strain decrease markedly after aging, indicating a reduction in its low-temperature ductility and crack resistance. The increased brittleness of the asphalt binder and reduced resistance to thermal shrinkage are attributed to oxidation reactions occurring during aging. As PMDI content increases from 0 % to 6 %, the peak stress of aged PhGAM/PMDI gradually decreases from 3.88 MPa to 3.59 MPa, while the corresponding strain increases from 3.2 % to 4.9 %. These results demonstrated that PMDI effectively mitigates the detrimental effects of aging on the cracking resistance of PhGAM, enhancing the mixture's toughness and ductility.

Fig. 13 illustrates the FE values of aged PhGAM/PMDI. It can be seen that the FE of aged PhGAM/PMDI gradually decreases with increasing PMDI content, while the rate of FE loss initially decreases sharply and then gradually stabilizes. Notably, the FE loss rates of PhGAM/PMDI4 and PhGAM/PMDI6 are similar, at approximately 23–24 %. The findings implied that the incorporation of 4 % PMDI into the binder significantly enhances the crack resistance of aged PhGAM/PMDI, while higher dosages provide minimal additional benefits. This is because an appropriate amount of PMDI is sufficient to enhance the structural stability of the asphalt binder at the molecular level, enhancing the toughness and FE of PhGAM, and helps mitigate the deterioration of low-temperature performance caused by aging and applied loads (Al Khateeb et al. 2024, Izquierdo et al. 2014).

3.4.2. Stiffness modulus

Fig. 14 reveals the stiffness modulus values of aged PhGAM/PMDI. After aging, the stiffness modulus of PhGAM/PMDI exhibits a differentiated increase, indicating that the stiffness of aged PhGAM/PMDI is higher than that of its unaged counterpart. With the increasing PMDI content, the stiffness modulus of aged PhGAM/PMDI initially decreases and then increases, reaching a minimum value of 1271.5 MPa at a PMDI content of 4 %. In addition, the rate of change in stiffness modulus before and after aging shows a similar trend, with PhGAM/PMDI4 exhibiting the lowest change rate of only 44 %. These results confirmed that PMDI enhances the low-temperature flexibility of aged PhGAM, with the greatest improvement achieved at 4 %, beyond which additional PMDI provides limited further benefit.

3.4.3. Macroscopic fracture morphology

Fig. 15 presents the macroscopic fracture morphology of unaged and aged PhGAM/PMDI obtained at low temperatures. Compared to unaged

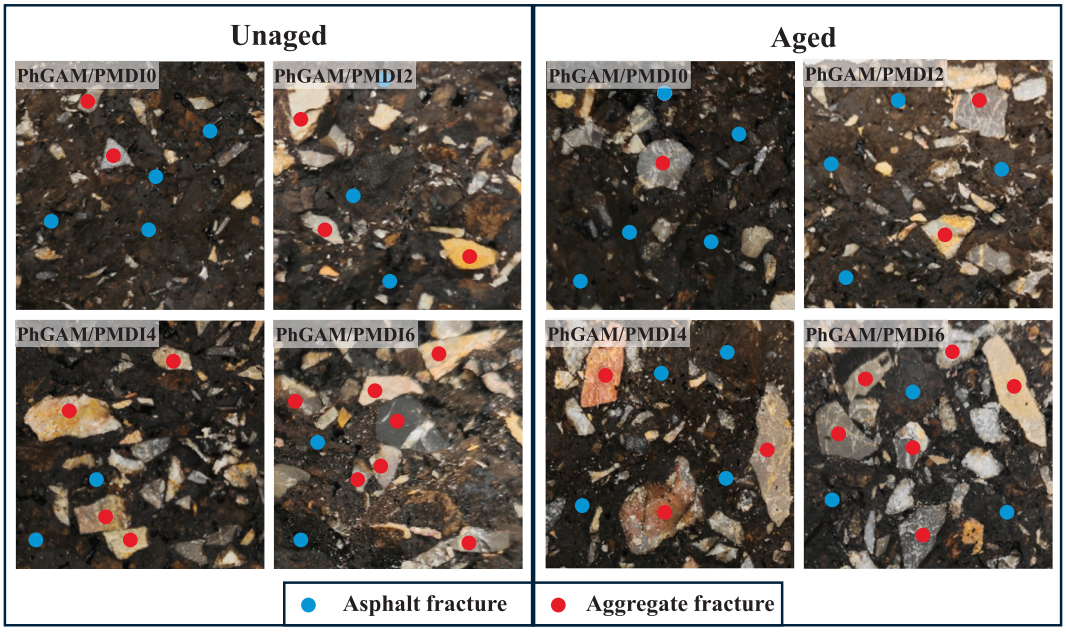

Fig. 15. Effect of aging on the macroscopic fracture morphology of PhGAM/PMDI.

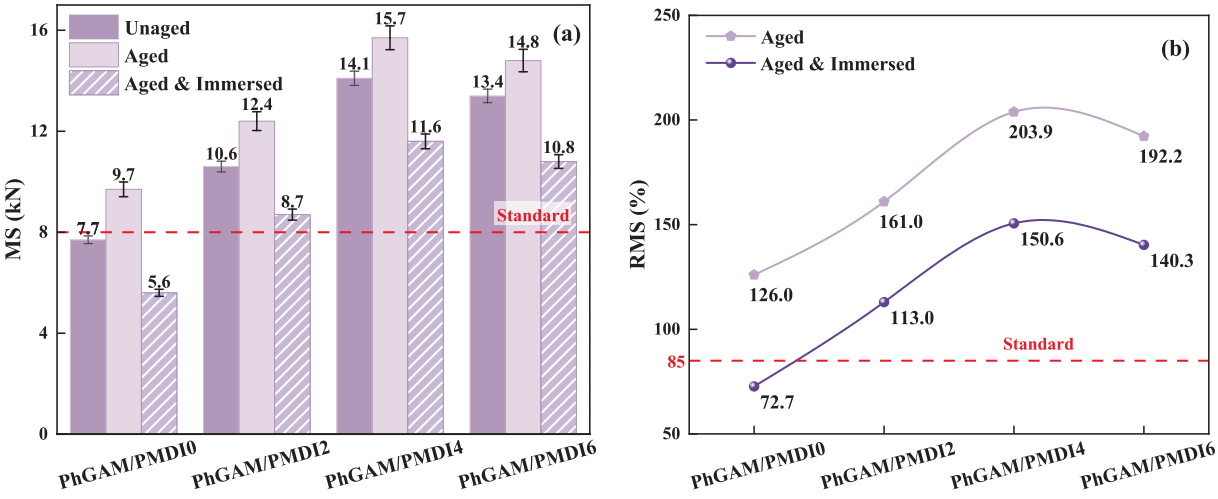

Fig. 16. Moisture-conditioned mechanical properties of aged PhGAM/PMDI: (a) MS and (b) RMS.

PhGAM, the aged PhGAM exhibits more pronounced fractures within the asphalt binder. With the increasing PMDI content, the fracture patterns shift from cohesive failure within the binder to adhesive failure involving aggregate fracture. This transition indicated a significant reduction in aging-related deterioration, thereby greatly enhancing the crack resistance of PhGAM. This is primarily due to the involvement of PMDI in chemical reactions within the asphalt binder, which enhances its low-temperature toughness and effectively mitigates embrittlement induced by aging. (Li, T. et al. 2021). Overall, PMDI significantly strengthens the interfacial adhesion of the binder to mineral aggregates, contributing to the observed shift in fracture mechanism from cohesive to adhesive failure.

3.5. Moisture-induced performance

3.5.1. Immersed MS

Fig. 16 depicts the Moisture-conditioned mechanical properties of aged PhGAM/PMDI. From Fig. 16(a), as PMDI is added from 0 % to 2 %, 4 %, and 6 %, the MS value of aged PhGAM increases from 9.7kN to 12.4kN, 15.7kN, and 14.8kN, representing approximate increases of 26 %, 15 %, and 10 %, respectively, compared to unaged PhGAM. These results suggested that the designed aging condition does not negatively affect the resistance of PhGAM to applied loads, and the embedded PMDI does not compromise this benefit. Furthermore, after further immersion, compared with unaged specimens, the MS value of aged PhGAM/PMDI0 dramatically decreases to 5.6 kN, falling below the required 8 kN, corresponding to a reduction of approximately 27 %. The MS values of PhGAM/PMDI2, PhGAM/PMDI4, and PhGAM/PMDI6 decrease to 8.7 kN, 11.6 kN, and 10.8 kN, respectively, corresponding to reductions of 18 %, 18 %, and 19 %. These findings demonstrated that an appropriate amount of PMDI, particularly at 4 %, effectively enhances the resistance of PhGAM to moisture-induced deterioration under aging-immersion coupling conditions, thereby contributing to improved long-term water stability.

Fig. 16(b) illustrates that the RMS values exhibit an increasing–then–decreasing trend with rising PMDI content, irrespective of immersion conditions. A PMDI dosage of 4 % results in the highest RMS value, reaching 203.9 % prior to immersion and remaining the

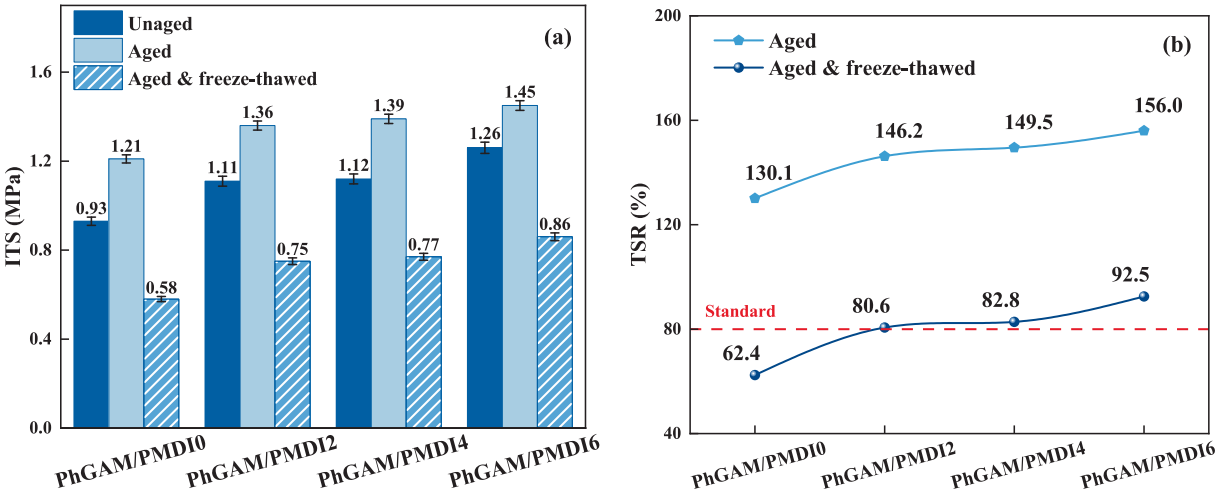

Fig. 17. Aged PhGAM/PMDI mechanical properties under freeze-thaw conditions: (a) ITS and (b) TSR.

maximum at 150.6 % after immersion. Notably, the RMS value of aged PhGAM/PMDI0 drops sharply to 72.7 % after immersion, failing to meet the required standard of 85 % and corresponding to a reduction of approximately 42 %. After the incorporation of 2 %, 4 %, and 6 % PMDI, the RMS values of PhGAM increase progressively to 113 %, 150.6 %, and 140.3 %, respectively. These results indicated that PhGAM alone has poor resistance to moisture damage, and the introduction of PMDI effectively overcomes this limitation, significantly improving the residual strength of PhGAM under aging-immersion coupling conditions, particularly at 4 % PMDI. This enhancement is primarily attributed to chemical reactions between the free –NCO groups in PMDI-modified asphalt and the –OH groups or water molecules on the surfaces of aggregates and PhG. Such interactions promote the formation of a cross-linked structure, which significantly enhances the adhesion between the asphalt binder and the aggregates (Xu et al. 2025).

3.5.2. F-T ITS

Fig. 17 exhibits the Aged PhGAM/PMDI mechanical properties under F-T conditions. According to Fig. 17(a), with the increase in PMDI content from 0 % to 6 %, PhGAM exhibits a consistent increasing trend in ITS values under unaged, aged, and aged-freeze-thawed conditions. Specifically, after aging, the ITS values of PhGAM/PMDI with PMDI contents of 0 %, 2 %, 4 % and 6 % are 1.21 MPa, 1.36 MPa, 1.39 MPa, and 1.45 MPa, which increased by about 30 %, 23 %, 24 % and 15 % compared to before aging. These results indicated that the designed aging conditions do not compromise the structural integrity of PhGAM, and the incorporation of PMDI does not adversely affect its structural stability. Furthermore, after further F-T conditioning, the ITS value of PhGAM/PMDI0 decreases to 0.58 MPa, approximately 38 % lower than the unaged value. With the addition of 2 %, 4 %, and 6 % PMDI, the ITS values of PhGAM are 0.75 MPa, 0.77 MPa, and 0.86 MPa, corresponding to reductions of approximately 32 %, 31 %, and 32 % relative to the unaged condition. These findings suggested that PhGAM alone has insufficient water stability and is prone to structural failure under aging-F-T coupling conditions, whereas PMDI enhances resistance to interfacial damage caused by expansion stresses from pore water freezing, thereby improving moisture resistance and long-term durability.

Fig. 17(b) clearly shows that the TSR value of aged PhGAM progressively increases as the PMDI content rises from 0 % to 6 %, with values changing from 130.1 % to 146.2 %, 149.5 %, and 156 %, representing approximate improvements of 12 %, 15 %, and 20 %, respectively. After F-T conditioning, the TSR value of PhGAM/PMDI0 significantly decreases to 62.4 % (falling below the required 80 %), with a reduction of approximately 52 %, whereas the TSR values of PhGAM with 2 %, 4 %, and 6 % PMDI incorporation are 80.6 %, 82.8 %, and 92.5 %, respectively. These findings indicated that PhGAM alone exhibits poor resistance to moisture-induced damage under coupled aging and F-T conditions, while the incorporation of PMDI effectively enhances F-T resistance and binder-aggregate adhesion under thermal expansion.

4. Summary and conclusions

PhG was employed as a complete replacement for conventional mineral filler, while PMDI was added as an asphalt binder modifier to prepare PhGAM/PMDI mixtures, aiming to enhance its overall engineering performance and durability. The SCB and F-T cycling tests were executed to characterize the fatigue performance and freeze-thaw (F-T) resistance of PhGAM/PMDI. In addition, a series of tests including wheel tracking, low-temperature ITS, MS, and F-T ITS were conducted to comprehensively evaluate the high-temperature performance, low-temperature cracking resistance, and moisture-induced deterioration resistance of aged PhGAM/PMDI. The major findings are detailed as follows:

- The SCB-based fatigue test results demonstrated that PMDI shows significant capacity to improve the resistance of PhGAM to fatigue, which works limitedly while exceeding 4 %. Beyond this, the use of PMDI does not increase the susceptibility of PhGAM to fatigue damage under repeated loading.
- The F-T cycling test results identified that PMDI brings significantly pronounced performance benefits to PhGAM in F-T resistance, enabling PhGAM/PMDI0 to withstand at least four F-T cycles with TSR values exceeding 75 %.
- The wheel tracking test illustrated that the PhGAM/PMDI mixtures work remarkedly to have the DS value increased for high-temperature stability benefits after thermo-oxidative aging, such as reaching a 5736 passes/mm for PhGAM/PMDI4, as compared to PhGAM/PMDI0 at 2921 passes/mm.
- The low-temperature test results indicated that PMDI can help mitigate the detrimental effects of aging on the cracking resistance of PhGAM with more adhesive failures at low temperatures, which is most effective in delaying reductions in flexibility and ductility when PMDI content is limited to 4 %.
- The after-aging based moisture-induced damage results suggested that 4 % PMDI greatly contributes to improving the aged/immersed and aged/F-T stabilities of PhGAM, with MS and RMS values of 11.6 kN and 150.6 %, and ITS and TSR values of 0.77 MPa and 82.2 %, while aged PhGAM/PMDI0 fails to meet applications with respective RMS and TSR values at 72.7 % and 62.4 %.

Overall, incorporating 4 % PMDI into the asphalt binder provides the most effective balance among fatigue resistance, high-temperature stability, low-temperature cracking resistance, and moisture resistance, thereby significantly enhancing the recycling potential of PhG as a filler. PMDI-modified asphalt binder is feasible for promoting the sustainable utilization of PhG in asphalt mixtures.

5. Limitations and future work

This study mainly focused on laboratory-scale evaluations, and field performance validation of PhGAM mixtures has not yet been conducted. Future research should involve field trials under diverse service conditions, along with life cycle assessment (LCA) and life cycle cost analysis (LCCA), to provide more robust evidence for the practical and long-term application of PhGAM.

CRediT authorship contribution statement

Xiaomei Huang: Writing – review & editing, Writing – original draft, Software, Methodology, Formal analysis, Data curation. **Xiong Xu:** Writing – review & editing, Writing – original draft, Validation, Supervision, Project administration, Funding acquisition, Conceptualization. **Guohao Xu:** Validation, Software, Methodology, Investigation, Data curation. **Xiong Tao:** Validation, Resources, Methodology. **Anand Sreeram:** Validation, Methodology, Formal analysis. **Zhifei Tan:** Writing – review & editing, Validation, Supervision, Investigation.

Declaration of competing interest

The authors declare that they have no known competing financial interests or personal relationships that could have appeared to influence the work reported in this paper.

Acknowledgements

The authors gratefully acknowledge the supports provided by the Science and Technology Plan Project of Department of Housing and Urban-Rural Development of Hubei Province (2023177), the National Natural Science Foundation of China (52408287), the International Science and Technology Cooperation Project of Hubei Province (2024EHA002), and the 16th Graduate Education Innovation Fund of Wuhan Institute of Technology (CX2024531).

Data availability

The data that has been used is confidential.

References

Al Khateeb, G.G., Alattieh, S.A., Zeiada, W., Castorena, C., 2024. State-of-the-art review on the behavior of bio-asphalt binders and mixtures. Molecules 29 (16), 3835.
Amrani, M., El Haloui, Y., Hajikarimi, P., Sehaqui, H., Hakkou, R., Barbachi, M., Taha, Y., 2020. Feasibility of using phosphate wastes for enhancing high-temperature rheological characteristics of asphalt binder. J. Mater. Cycles Waste Manag. 22, 1407–1417.
Arbabpour Bidgoli, M., Naderi, K., Moghadas Nejad, F., 2019. Effect of filler type on moisture susceptibility of asphalt mixtures using mechanical and thermodynamic properties. J. Mater. Civ. Eng. 31 (4), 04019024.
Baolin, K., Qin, Z., Xianhai, L., Zhihui, S., 2022. Adsorption and solidification of cadmium by calcium sulfate dihydrate (gypsum) in an aqueous environment: A dispersion-corrected DFT and ab initio molecular dynamics study. PCCP 24 (16), 9521–9533.
Bilal, E., Bellefqih, H., Bourgier, V., Mazouz, H., Dumitraş, D.G., Bard, F., Laborde, M., Caspar, J.P., Guilhot, B., Iatan, E.L., 2023. Phosphogypsum circular economy considerations: A critical review from more than 65 storage sites worldwide. J. Clean. Prod. 414, 137561.
Bui, H.H., Saleh, M., 2021. Effects of specimen size and loading conditions on the fracture behaviour of asphalt concretes in the SCB test. Eng. Fract. Mech. 242, 107452.
Cao, J., Wang, Z., Ma, X., Yang, X., Zhang, X., Pan, H., Wu, J., Xu, M., Lin, L., Zhang, Y., 2022. Promoting coordinative development of phosphogypsum resources reuse through a novel integrated approach: A case study from China. J. Clean. Prod. 374, 134078.
Cao, Z., Chen, M., Yu, J., Han, X., 2020. Preparation and characterization of active rejuvenated SBS modified bitumen for the sustainable development of high-grade asphalt pavement. J. Clean. Prod. 273, 123012.
Chen, J.-S., Kuo, P.-H., Lin, P.-S., Huang, C.-C., Lin, K.-Y., 2008. Experimental and theoretical characterization of the engineering behavior of bitumen mixed with mineral filler. Mater. Struct. 41 (6), 1015–1024.
Chen, J., Chen, K., Liu, Z., 2024. Research on the expansion, shrinkage properties and fracture evolution of red clay stabilised with phosphogypsum under dry-wet cycles. PLoS One 19 (8), e0308616.
Chen, Y., Xu, S., Tebaldi, G., Romeo, E., 2022. Role of mineral filler in asphalt mixture. Road Mater. Pavement Des. 23 (2), 247–286.
Cheng, Y., Tao, J., Jiao, Y., Tan, G., Guo, Q., Wang, S., Ni, P., 2016. Influence of the properties of filler on high and medium temperature performances of asphalt mastic. Constr. Build. Mater. 118, 268–275.
Gao, L., Ni, F., Ling, C., Yan, J., 2016. Evaluation of fatigue behavior in cold recycled mixture using digital image correlation method. Constr. Build. Mater. 102, 393–402.
Gong, X., Liu, Q., Chen, P., Wang, H., Liu, X., Chen, S., Wu, S., 2024. Modification mechanism of green polyurethane modified asphalt prepared by in-situ polymerization. Constr. Build. Mater. 448, 138243.
Izquierdo, M., García Morales, M., Martínez Boza, F., Navarro, F., 2014. Thermo-mechanical properties and microstructural considerations of MDI isocyanate-based bituminous foams. Mater. Chem. Phys. 146 (3), 261–268.
Jiang, W., Zhang, M., Ren, P., Xing, C., Yuan, D., Wu, W., 2024. Development of porous asphalt mixture based on the synthesis of PTEMG and MDI polyurethane asphalt. Constr. Build. Mater. 411, 134537.
Jin, Q., Wang, L., Ren, Z., Li, X., Liu, S., 2025. Effect of modified phosphogypsum on the dimensional stability of supersulfated cement-based materials. Case Stud. Constr. Mater. 22, e04170.
Khairuddin, F.H., Alamawi, M.Y., Yusoff, N.I.M., Badri, K.H., Ceylan, H., Tawil, S.N.M., 2019. Physicochemical and thermal analyses of polyurethane modified bitumen incorporated with Cecabase and Rediset: Optimization using response surface methodology. Fuel 254, 115662.
Li, T., Carreño Gómez, N.H., Lu, G., Liang, D., Wang, D., Oeser, M., 2021a. Use of polyurethane precursor–based modifier as an eco-friendly approach to improve performance of asphalt. J. Transp. Eng. Part B Pavements 147 (3), 04021031.
Li, Z., Yang, F., Yuan, J., Cong, L., Yu, M., 2021b. Study on preparation and pavement performance of polyurethane modified asphalt based on in-situ synthesis method. Constr. Build. Mater. 309, 125196.
Liang, Y., Bai, T., Zhou, X., Wu, F., Chenxin, C., Peng, C., Fuentes, L., Walubita, L.F., Li, W., Wang, X., 2023. Assessing the effects of different fillers and moisture on asphalt mixtures' mechanical properties and performance. Coatings 13 (2), 288.
Liu, G., Guan, B., Liang, Y., Xing, H., Huang, A., Qin, J., 2022. Preparation of phosphogypsum (PG) based artificial aggregate and its application in the asphalt mixture. Constr. Build. Mater. 356, 129218.
Luo, Y., Huang, J., Wang, Y., Hu, T., Xu, X., Yin, B., 2025. Enhancing the properties and engineering performance of asphalt binders and mixtures with physicochemically treated waste wind turbine blades. Constr. Build. Mater. 473, 141023.
Mehta, S., Pastariya, S., Bhargava, A., Verma, G., Bharadwaj, A., 2020. Bitumen concrete mix design using cement and phosphogypsum as filler materials. Int. J. Adv. Eng. Res. Sci. 7 (6), 296–300.
Murali, G., Azab, M., 2023. Recent research in utilization of phosphogypsum as building materials. J. Mater. Res. Technol. 25, 960–987.
Ou, L., Li, R., Zhu, H., Zhao, H., Chen, R., 2023. Upcycling waste phosphogypsum as an alternative filler for asphalt pavement. J. Clean. Prod. 420, 138332.
Pereira, L., Freire, A., da Costa, M.S., Antunes, V., Quaresma, L., Micaelo, R., 2018. Experimental study of the effect of filler on the ductility of filler-bitumen mastics. Constr. Build. Mater. 189, 1045–1053.
Qu, F., Zhang, Y., Li, M., Dong, W., Li, W., Tsang, D.C., 2025. Resource recycling of industrial waste phosphogypsum in cementitious materials: Pretreatment, properties, and applications. J. Environ. Manage. 376, 124291.
Shi, X., Zeng, A., Duan, H., Zhang, H., Yang, J., 2024. Status and development trends of phosphogypsum utilization in China. Circular Econ 3 (4), 100116.
Sun, Q., Tao, L., Li, X., Xu, W., Yao, S., Li, J., Ren, Q., Chen, Y., Xu, C., Wu, Z., 2023. Study on preparation of inorganic binder stabilized material with large dosage of phosphogypsum. J. Korean Ceram. Soc. 60 (6), 883–895.
Tan, Z., Guo, Y., Hu, G., Chen, R., Wang, Y., Yin, B., Leng, Z., 2025. Upcycling waste wind turbine blades into fiber-reinforced asphalt mortar: A chemical recycling approach and performance assessment. Constr. Build. Mater. 489, 142352.
Teixeira, J.E.S.L., Junior, C.M.A., de Rezende, L.R., Branco, V.T.F.C., Kim, Y.R., 2023. Evaluation of asphalt concrete's fatigue behavior using cyclic semi-circular bending test. Constr. Build. Mater. 400, 132772.
Wang, H., Al-Qadi, I.L., Faheem, A.F., Bahia, H.U., Yang, S.-H., Reinke, G.H., 2011. Effect of mineral filler characteristics on asphalt mastic and mixture rutting potential. Transp. Res. Rec. 2208 (1), 33–39.
Woszuk, A., Bandura, L., Franus, W., 2019. Fly ash as low cost and environmentally friendly filler and its effect on the properties of mix asphalt. J. Clean. Prod. 235, 493–502.
Wu, W., Jiang, W., Yuan, D., Lu, R., Shan, J., Xiao, J., Ogbon, A.W., 2021. A review of asphalt-filler interaction: Mechanisms, evaluation methods, and influencing factors. Constr. Build. Mater. 299, 124279.
Xia, L., Cao, D., Zhang, H., Guo, Y., 2016. Study on the classical and rheological properties of castor oil-polyurethane pre polymer (C-PU) modified asphalt. Constr. Build. Mater. 112, 949–955.

Xing, B., Fang, C., Lyu, X., Fan, W., Lyu, Y., 2024. Influence of mineral filler characteristics on the filler–asphalt interfacial behavior. Adv. Powder Technol. 35 (10), 104636.
Xu, P., Chen, Z., Cai, J., Pei, J., Gao, J., Zhang, J., Zhang, J., 2019. The effect of retreated coal wastes as filler on the performance of asphalt mastics and mixtures. Constr. Build. Mater. 203, 9–17.
Xu, X., Leng, Z., Lan, J., Wang, W., Yu, J., Bai, Y., Sreeram, A., Hu, J., 2021. Sustainable practice in pavement engineering through value-added collective recycling of waste plastic and waste tyre rubber. Engineering 7 (6), 857–867.
Xu, X., Sreeram, A., Leng, Z., Yu, J., Li, R., Peng, C., 2022. Challenges and opportunities in the high-quality rejuvenation of unmodified and SBS modified asphalt mixtures: State of the art. J. Clean. Prod. 378, 134634.
Xu, X., Xu, G., Huang, X., Alam, G.B., Chen, X., Sreeram, A., 2025. Material characterization and engineering performance evaluation of phosphogypsum as a high-performance filler for bituminous pavements. Fuel 393, 134977.
Yin, P., Pan, B., Li, Z., Jiao, B., Liu, Y., 2024. Effect of surfactant modified phosphogypsum whisker on service performance of asphalt based on multi-scale experiments. J. Clean. Prod. 464, 142774.
Zhang, J., Liu, S., Yao, Z., Wu, S., Jiang, H., Liang, M., Qiao, Y., 2018. Environmental aspects and pavement properties of red mud waste as the replacement of mineral filler in asphalt mixture. Constr. Build. Mater. 180, 605–613.
Zhang, L., Mo, K.H., Tan, T.H., Yong, C.L., Yap, S.P., Lee, F.W., 2025a. Role of hydrogen peroxide and sodium lauryl sulfate in producing fiber-reinforced lightweight foamed phosphogypsum-based material. Mater. Reports: Solidwaste Ecomater. 1, 9520011.
Zhang, M., Xiong, K., Zhang, J., Li, Y., He, Y., Pei, J., 2024. Evaluation of the rheological properties and aging resistance of asphalt modified by MDI/TDI polyurethane. Constr. Build. Mater. 411, 134350.
Zhang, X., Zhang, J., Li, J., Zhu, H., Ou, L., Shan, B., 2025b. Rheological and anti-aging properties of modified asphalt with surface-modified calcium sulfate whiskers. Constr. Build. Mater. 489, 142205.
Zhang, Z., Liu, H., Zhu, Y., Chen, L., Sun, J., Wang, L., Huang, T., 2025c. Modification of bitumen with polyether-based polyurethanes containing different hard segments. J. Traffic. Transp. Eng. (eng Ed) 12 (2), 344–360.